



Contents lists available at ScienceDirect

# Ocean Modelling

journal homepage: [www.elsevier.com/locate/ocemod](http://www.elsevier.com/locate/ocemod)

## Two-way coupling of an ENSO model to the global climate model CLIMBER-3 $\alpha$

Heiko Goelzer\*, Anders Levermann, Stefan Rahmstorf

Potsdam Institute for Climate Impact Research, Potsdam, Germany  
 Potsdam University, Potsdam, Germany

### ARTICLE INFO

#### Article history:

Received 30 January 2008

Received in revised form 13 March 2009

Accepted 14 March 2009

Available online 25 March 2009

#### Keywords:

EMIC

ENSO

Coupled model

### ABSTRACT

We present a model study that investigates to what extent it is possible to introduce ENSO variability to an Earth system Model of Intermediate Complexity (EMIC). The Zebiak–Cane ENSO model is dynamically coupled to the EMIC CLIMBER-3 $\alpha$ , which by itself exhibits no interannual or multidecadal variability. ENSO variability is introduced to CLIMBER-3 $\alpha$  by adding ENSO-related sea surface temperature anomalies to the upper layers of the model ocean. For the other coupling direction, changes in the mean CLIMBER-3 $\alpha$  climate on decadal time scales are used to change the background state of the ENSO model, achieving a two-way coupling. We compare typical ENSO-related patterns of a fully coupled pre-industrial model run to reanalysis data and point out the possibilities and limitations of this model configuration. Although introduced ENSO-related SST anomalies and other related variables like the Southern Oscillation Index are well reproduced by the EMIC in the forcing domain, teleconnections to other regions are damped, especially in meridional direction. The reason for this limitation is the atmospheric model, which does not sufficiently resolve the necessary transport mechanisms. Despite this limitation the presented coupling method may still be a useful tool in combination with higher resolution atmospheric models as being in development for the successor model CLIMBER-3 and possibly other EMICs.

© 2009 Elsevier Ltd. All rights reserved.

### 1. Introduction

In recent years the mechanism of El Niño/Southern Oscillation (ENSO) has been extensively studied in a range of model setups, starting from strongly simplified conceptual models via local models of the Tropical Pacific to comprehensive General Circulation Models (GCMs) that explicitly resolve ENSO dynamics. Since Bjerknes (1969), conceptual models have been used to propose the basic, large scale feedback mechanisms dominating ENSO oscillations (Suarez and Schopf, 1988; Battisti and Hirst, 1989; Jin, 1997; Picaut et al., 1997; Wang, 2001). Local coupled models of the Tropical Pacific such as the Zebiak–Cane model (Zebiak and Cane, 1987; Battisti, 1988) have been used to test conceptual hypotheses and have added considerably to the understanding of ENSO mechanisms. They are now widely used to predict ENSO events with a lead time of several months (e.g. Chen et al. (2004)). Although this class of models has proven successful in reproducing the important physical mechanisms at play, they lack the global dimension by design and cannot be used on their own to study connections to other climate subsystems.

The quality of simulation of ENSO with GCMs has improved in recent years (AchutaRao and Sperber, 2006) making them valuable

tools for the study of ENSO dynamics. Nevertheless, comprehensive GCMs at sufficient resolution for ENSO are still too costly for simulations of considerably different climates (e.g. the last glacial maximum) where data is sparse and equilibrium simulations are needed. Because of the high computational costs, GCM model runs cannot be used for systematic sensitivity analyses of model parameters, which is a typical application for models of lower resolution like the one we are using here.

In this study we couple the Earth system model of intermediate complexity (EMIC) CLIMBER-3 $\alpha$  with the dynamical Zebiak–Cane ENSO model (ZC) (Zebiak and Cane, 1987). We investigate how far the coupled model can reproduce the ENSO dynamics and teleconnections to other climate subsystems. A precursor of our model setup, namely a one-way coupling, was used by Timmermann et al. (2005) to study a shoaling of the thermocline due to a collapse of the thermohaline circulation (THC) and its influence on ENSO. Timmermann et al. (2005) use their EMIC to uni-directionally couple changes in its background state into the ENSO model. For a more general study of the influence of changes in the background state on ENSO in the ZC, see Tziperman et al. (1997).

We extend the setup and couple both ways by additionally introducing ENSO variability to the EMIC (Fig. 1). On the one hand, changes in the long-term climate state of the EMIC enter the ZC by supplying anomalies to its background state. On the other hand, the SST of the EMIC, which by itself exhibits no interannual or multidecadal variability, is perturbed by SST anomalies as calculated by the ZC. The coupling between the EMIC and the ENSO model

\* Corresponding author. Present address: Departement Geografie, Vrije Universiteit Brussel, Pleinlaan 2, 1050 Brussel, Belgium. Tel.: +32 2 629 3782; fax: +32 2 629 3378.

E-mail address: [heiko.goelzer@vub.ac.be](mailto:heiko.goelzer@vub.ac.be) (H. Goelzer).

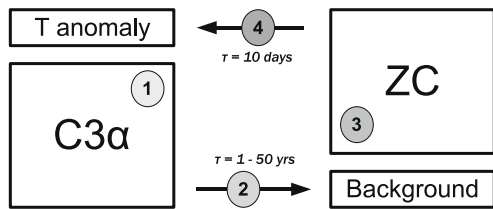


**Fig. 1.** Model components and coupling configuration: (1) CLIMBER-3 $\alpha$  model, (2) modification of the ZC background state, (3) ZC model, (4) modification of CLIMBER-3 $\alpha$  SST. Also given are the two distinct coupling time constants.

is thus distinct for both coupling directions and is applied on distinct time scales. Sensitivity of the ENSO model to changes in the mean climate state can be studied by control over the varying background state (2 in Fig. 1). If the coupling is successful, control over the SST coupling (4 in Fig. 1) would allow to study the effects of ENSO variability in the global model and interconnections to other climatic subsystems.

Next we describe the models and the two distinct coupling processes (Section 2), followed by results of a coupled model equilibrium simulation of pre-industrial climate and its comparison with observational data (Section 3). Finally we discuss in Section 4 the applicability of the presented hybrid model.

## 2. Model description

### 2.1. The EMIC CLIMBER-3 $\alpha$

The coupled atmosphere–ocean Earth system model of intermediate complexity CLIMBER-3 $\alpha$  consists of an oceanic general circulation model (GCM) based on the GFDL MOM-3 code (Pacanowski and Griffies, 1999) coupled to an interactive atmosphere (Petoukhov et al., 2000; Ganopolski et al., 2001) and a dynamic–thermodynamic sea ice module (Cheeto and Maqueda, 1997). The horizontal resolution of the ocean model is  $3.75^\circ \times 3.75^\circ$  with 24 vertical levels and the oceanic timestep is 12 h. The model utilizes an advection scheme with low numerical diffusivity (Hofmann and Maqueda, 2006; Prather, 1986). In our version, the background vertical diffusivity is set to  $0.3 \cdot 10^{-4} \text{ m}^2/\text{s}$ . A detailed description of the model can be found in Montoya et al. (2005) and sensitivity studies to changes in Southern ocean winds and vertical diffusivity in Levermann et al. (2007) and Mignot et al. (2006). In order to improve the model's performance for pre-industrial climate, we use a slightly modified model version: Isopycnal diffusivity was doubled to  $2000 \text{ m}^2/\text{s}$ . The topography was deepened in order to increase the Indonesian throughflow. And furthermore, Trenberth et al. (1989) wind stress data is used for the wind stress anomaly model compared to NCEP reanalysis data as in the standard configuration. These changes enhance and deepen the Atlantic meridional overturning circulation and cause a more realistic surface salinity distribution. The zonally integrated Atlantic streamfunction exhibits a maximum value of about 17 Sv with 13 Sv Southern Ocean outflow, consistent with observations (Talley et al., 2003; Ganachaud and Wunsch, 2000). This improved model version was already used in Montoya and Levermann (2008) and Schewe and Levermann (accepted for publication) and details about the changes can be found there.

The atmospheric POTSDAM-2 model (Petoukhov et al., 2000; Ganopolski et al., 2001) has a coarse horizontal resolution ( $7.5^\circ$  in latitude and  $22.5^\circ$  in longitude) and is based on the assumption of a universal vertical structure of temperature and humidity, which allows to reduce the three-dimensional description to a set of two-dimensional prognostic equations for temperature and humidity. The pressure and velocity fields are diagnostic. The description of atmospheric dynamics is based on a quasi-geo-

strophic approach and a parameterization of the zonally averaged meridional atmospheric circulation. The synoptic processes are parameterized as diffusion terms with a turbulent diffusivity computed from atmospheric stability and horizontal temperature gradients. Compared with the standard version (Montoya et al., 2005), a damping term for the tropical sea level pressure (SLP) was removed. This has direct consequences for evaporation (E) and precipitation (P), which are now generally stronger in the Tropics. The term had been introduced earlier because of numerical instability which is not a problem in the current version.

Heat and freshwater fluxes between the ocean and the atmosphere are computed on the oceanic grid and applied without any flux adjustments. The wind stress however is computed as the sum of the Trenberth wind stress climatology (Trenberth et al., 1989) and the wind stress anomaly calculated by the atmospheric model relative to the control simulation. Thus, the wind stress forcing does not vary during equilibrium simulations. The original global model exhibits no synoptic, interannual or multi-decadal variability.

### 2.2. The Zebiak–Cane ENSO model

To introduce ENSO variability we couple the ZC ENSO model (Zebiak and Cane, 1987), a local coupled atmosphere–ocean model for the Tropical Pacific, to CLIMBER-3 $\alpha$ . Its oceanic part is simulated by a reduced gravity model and the atmospheric part is a type of Gill model (Gill, 1982), which has been extended with a parameterized moisture convergence feedback. The time evolution of the sea surface temperature (SST) is determined by horizontal advection, upwelling and heat loss to the atmosphere. It is computed on the atmospheric grid in a region  $129.375^\circ\text{E} - 275.625^\circ\text{E}$ ,  $19^\circ\text{S} - 19^\circ\text{N}$  which is also the domain used for coupling to CLIMBER-3 $\alpha$  (gray area in Fig. 2, left panel). The ZC timestep is 10 days.

The ZC operates as an anomaly model which computes the time evolution of deviations from a given background state. In its usual application as an ENSO prediction model, the background state results from a spin-up with historical wind data and current climate conditions (Chen et al., 2004). Thus, a background state with ocean currents that are consistent with the wind stress forcing is produced, which is then held constant during the course of the prediction.

In our setup, the spin-up is done with a climatology of long-term mean NCEP reanalysis wind data (Kalnay et al., 1996) and Reynolds and Smith SST (Reynolds and Smith, 1994) which is used as boundary condition in the NCEP reanalysis model. In transient experiments, the background state might change due to variability of the EMIC. In this case, long-term mean anomalies of the EMICs variables are added to the NCEP climatology before the spin-up.

### 2.3. ENSO to EMIC coupling: introduction of SST variability

In order to introduce ENSO variability to CLIMBER-3 $\alpha$ , ZC SST anomalies are supplied to the ocean model by adding a heat source term to the tracer equation. The ZC calculates SST tendency terms (differences between last and current timestep anomalies) to account for zonal and meridional advection, upwelling and loss of heat to the atmosphere separately.

$$SST_t - SST_{t-1} = \Delta T_{adv(zon)} + \Delta T_{adv(mer)} + \Delta T_{upwelling} + \Delta T_{heatloss} \quad (1)$$

When supplying SST anomalies to CLIMBER-3 $\alpha$ , we omit  $\Delta T_{heatloss}$  because the coupled EMIC will respond to the oceanic anomaly with anomalous heat flux to the atmosphere by itself. This step is crucial for a good reproduction of the ENSO-related SST anomaly. The resulting tendency term is interpolated and masked to fit the CLIMBER-3 $\alpha$  grid domain (See gray shade in Fig 2, left panel). It is held constant

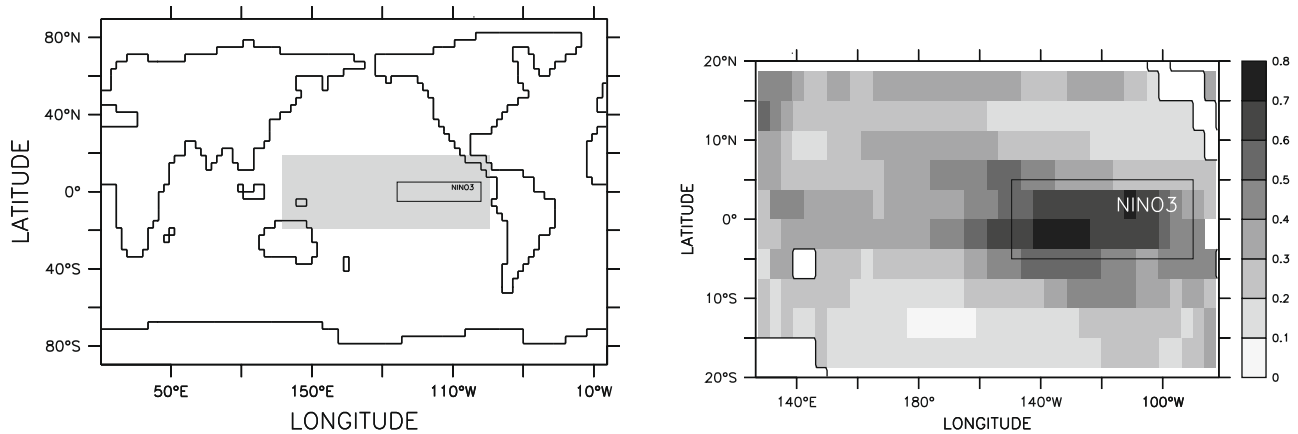


**Fig. 2.** Left: ZC model domain where SST anomalies are calculated with defined values in the region 129.375°E–275.625°E, 19°S–19°N (gray area). The Nino3 region (210°E–270°E) is marked as well. Right: RMS values for SST anomaly deviation from the ZC expectation in K.

during one ZC timestep of 10 days and is applied to the ocean with the corresponding scaling for each 12h timestep. The depth ( $h_F$ ) to which anomalies are supplied was set to  $h_F = 75$  m (upper 3 levels of the oceanic grid of CLIMBER-3 $\alpha$ ), close to the mixed layer depth given in ZC by 50 m. The depth difference between the two models shows that more heat input to CLIMBER-3 $\alpha$  is necessary in order to reproduce the SST variability in the ZC. This is due to the fact that part of the imposed heat anomaly is lost to the deeper ocean. To guarantee thermal energy conservation in the model, the upper level source term is balanced per timestep in deeper ocean layers. This is a crude approximation to the realisation of heat transport in the real ocean due to ENSO dynamics which cannot be resolved in a coarse model. The integral heat content that was added to the mixed layer is subtracted uniformly on the entire ZC domain between depth  $h_F = 75$  m and  $h_B = 700$  m in CLIMBER-3 $\alpha$ . The values for  $h_F$  and  $h_B$  were chosen in trial runs to minimize the average root mean square (RMS) value of SST anomaly deviation from the ZC expectation in the entire ZC region (Fig. 2, right panel).

$$\text{RMS} = \frac{1}{A_{\text{ZC}}} \cdot \int_{A_{\text{ZC}}} dx dy \sqrt{\frac{1}{n} \sum_{t=1}^n (\text{SST}_{\text{c3a}}(x, y, t) - \text{SST}_{\text{zc}}(x, y, t))^2}, \quad (2)$$

where  $n$ , the number of 10 day timesteps is in the order of 1000. The highest deviations appear in the central Tropical Pacific, where the EMIC exhibits generally lower temperatures than ZC during El Niño. The average SST anomaly in the Nino3 region (NINO3, 210°E–270°E, 5°S–5°N) in ZC and in the forced CLIMBER-3 $\alpha$  show very good agreement (Fig. 3).

The given scheme implies that SST anomalies would be the same in both models, if there were no differences in advection and heat loss to the atmosphere. This cannot be the case, given the different model configurations. Nevertheless, variability of the SST field and key features of the ENSO cycle are well reproduced in the EMIC.

We compare the induced heat flux to the ocean in both models (Fig. 4) which is generally negative during El Niño when the anomalously warm surface ocean loses heat to the atmosphere. In ZC the heat loss (solid in Fig. 4) takes the form of a linear damping term which is defined relative to the SST anomaly. Indeed the oceanic heat loss of the EMIC (dotted) reproduces the ZC variability very well. It is now the dominant mode of variability of the global heat flux at the ocean–atmosphere boundary (dashed), since the model does not include other modes of internal climate variability. The good representation of ZC variability in the EMIC is an encouraging result, as it proves the principal concept of introducing SST variability successful.

#### 2.4. EMIC to ENSO-model coupling: modification of the ZC background state

Changes in the CLIMBER-3 $\alpha$  climate state enter the ZC by modifications of its background state. The ZC background state on which anomalies are calculated is defined by fields for SST ( $T$ ), thermocline depth ( $h$ ), surface winds ( $\mathbf{u}^{\text{atm}}$ ) and wind divergence ( $\nabla \cdot \mathbf{u}^{\text{atm}}$ ) and internal fields for the horizontal surface currents ( $\mathbf{u}^{\text{oce}}$ ) and upwelling ( $\mathbf{w}^{\text{oce}}$ ). Changes in  $T$ ,  $h$ ,  $\mathbf{u}^{\text{atm}}$  and  $\nabla \cdot \mathbf{u}^{\text{atm}}$  can be directly diagnosed from CLIMBER-3 $\alpha$ . The internal fields ( $\mathbf{u}^{\text{oce}}$ ,  $\mathbf{w}^{\text{oce}}$ ) are produced by a separate run of the ZC with a given external background state and wind stress forcing ( $\tau$ ) which reaches equilibrium after 30 years. This is comparable to the standard spin-up procedure when ZC is used for ENSO predictions. The complete background state for the ZC model can be generated for a set of given  $T$ ,  $h$ ,  $\mathbf{u}^{\text{atm}}$  and  $\tau$  fields. Monthly mean anomalies of these fields are taken from the EMIC, interpolated to the ZC grid and added to NCEP long-term mean data as background to the ZC model. The thermocline depth  $h$  is calculated following Gnanadesikan (1999):

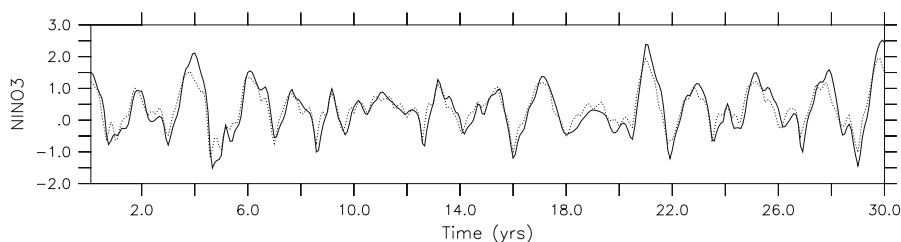


**Fig. 3.** ZC (solid) and forced CLIMBER-3 $\alpha$  (dotted) NINO3 time series in comparison.

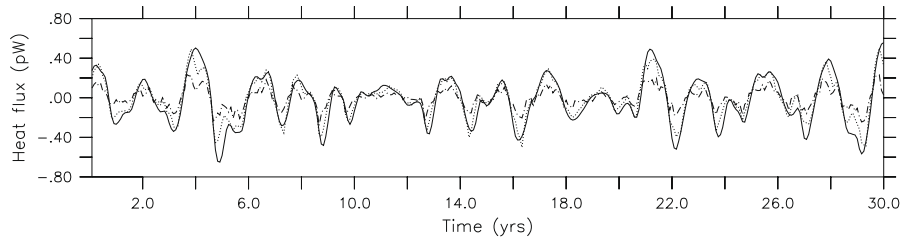


Fig. 4. ZC (solid) and CLIMBER-3 $\alpha$  (dotted) heat flux over the entire ZC region. CLIMBER-3 $\alpha$  global heat flux variability (dashed) is dominated by the ENSO-related part.

$$h = \int_{-H}^0 dz \Delta T \cdot z / \int_{-H}^0 dz \Delta T, \quad (3)$$

where  $H$  is the ocean depth,  $T(z)$  is the temperature and  $\Delta T = T(z) - T(max)$ . Levermann and Griesel (2004) showed that in CLIMBER-3 $\alpha$  the Atlantic  $h$  is not sensitive to perturbations of surface buoyancy flux.  $h$  however does vary with surface wind stress (Schewe and Levermann, accepted for publication). The background state should not include interannual variations, i.e. variability induced by the ZC itself. Therefore, the background states have to be temporally smoothed with a time constant considerable longer than the ENSO period. This is done by a running mean filter

$$B_i = \frac{1}{\tau_d} \sum_{k=i-\tau_d}^{i-1} B_k, \quad (4)$$

where  $B_k$  is the background state of year  $k$  and  $\tau_d$  is a fixed window size in years. The resulting  $B_i$  are long-term monthly mean values and represent the time-averaged seasonal cycle for the variables  $T$ ,  $h$ ,  $\mathbf{u}^{atm}$  and  $\nabla \cdot \mathbf{u}^{atm}$ . The applied temporal filter implies that variability on time scales shorter than  $\tau_d$  are damped.

### 3. Pre-industrial coupled climate state

#### 3.1. ENSO in CLIMBER-3 $\alpha$

We analyze the performance of the fully coupled model under pre-industrial conditions and compare with NCEP reanalysis data. We focus on how tropical SST anomalies influence other model variables and if that leads to ENSO-related teleconnections.

It is a well known fact that the ZC can show chaotic behavior with intermittent periods for several decades (Jin, 1997; Neelin et al., 1998). In the coupled model variability is reduced to a steady

seasonal cycle with persistent positive SST anomalies during these periods (Fig. 5). Being based on the chaotic behavior of the ZC, such phases appear unpredictable. We could not find a clear relation between the time constant of the background filter and the appearance of chaotic behavior. But, as it was not present when the background states were smoothed with a time constant of  $\tau_d = 50$  years, this value was chosen for the following experiments.

To compare model and data, we calculate the linear regression between time series of NINO3 and different variables at every grid point for both model and NCEP data and display the regression slope. Grid points are only considered where the correlation  $\rho$  is significant at a 95% level. For the test of the null hypothesis  $\rho = 0$  via the  $t$ -distribution, serial correlation was taken into account by estimating the effective degrees of freedom (von Storch and Zwiers, 1999, see, e.g.).

The resulting figures represent the ENSO-related patterns of the variable in question and show the change of the variable for a change of NINO3 by one. Although the ENSO cycle is not really symmetrical, the patterns may tentatively be interpreted as El Niño (or negative La Niña) climate signal.

The ENSO-related SST pattern (Fig. 6) represents the primary forcing to which other model variables, like surface air temperature (SAT), SLP and precipitation respond. Compared to reanalysis data which shows SST teleconnections to the extratropical Pacific and the Southern Ocean, the pattern in the model is confined to a strong warming signal in the eastern and central Tropical Pacific.

The atmosphere adjusts to the SST warming signal with a warmer SAT and a thermodynamic response of SLP, surface winds and vertical velocity (Fig. 7). Note that these fields are unrealistically wide due to the coarse atmospheric model resolution. The wind field is in reality much more localized and focused on the center of maximum surface warming.

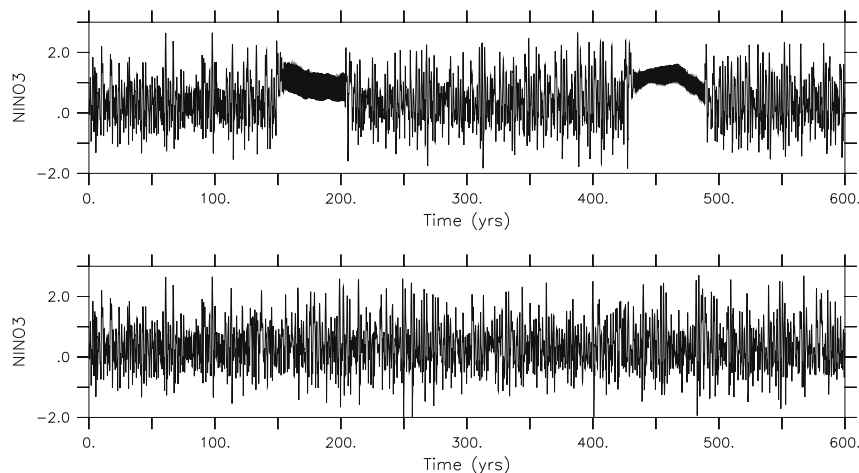


Fig. 5. NINO3 with intermittent periods. The background was filtered with a running mean window of  $\tau_d = 30$  (top) and  $\tau_d = 50$  (bottom) years.

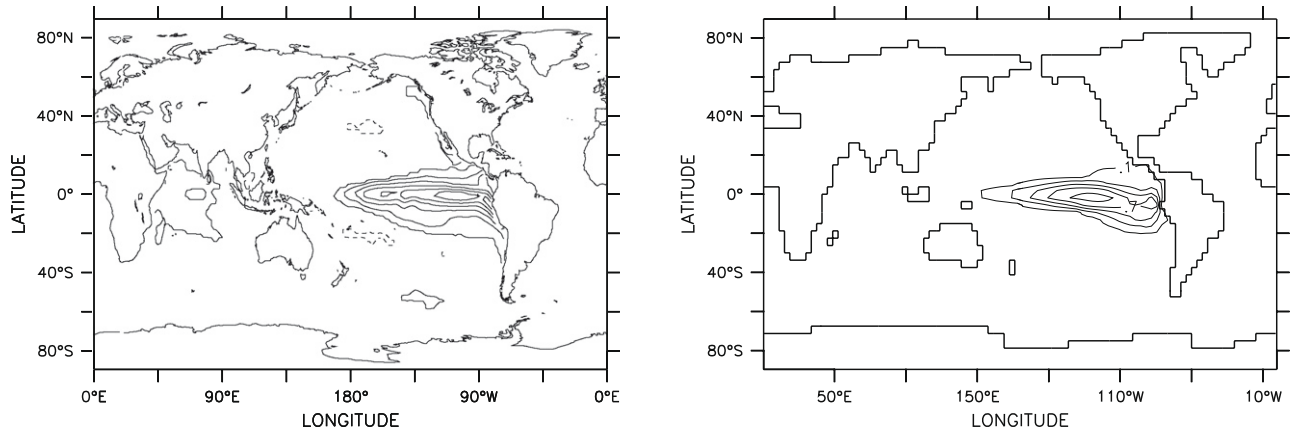


Fig. 6. Regression pattern between SST and NINO3 for NCEP (left) and Model (right). Contour interval is 0.2 °C.

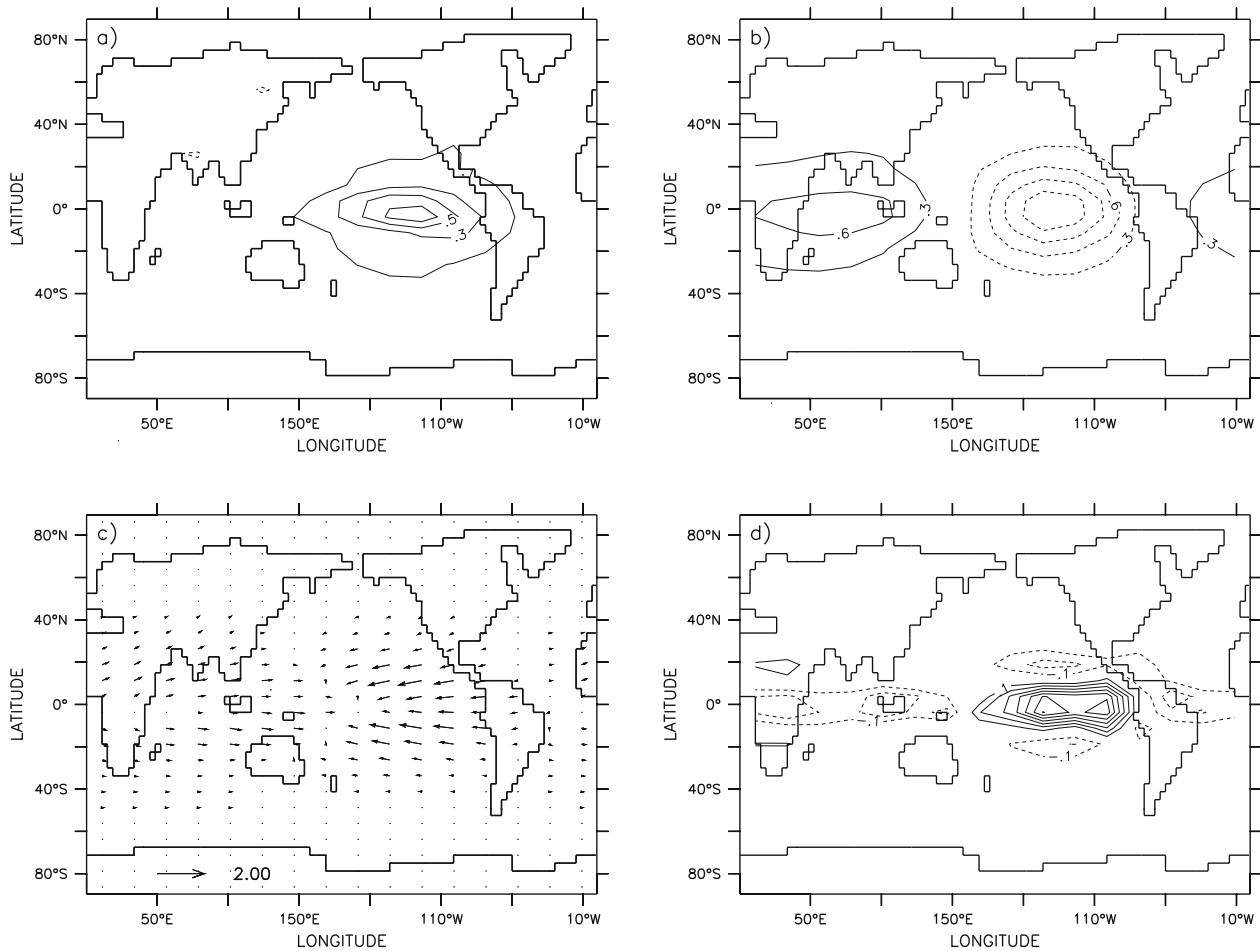
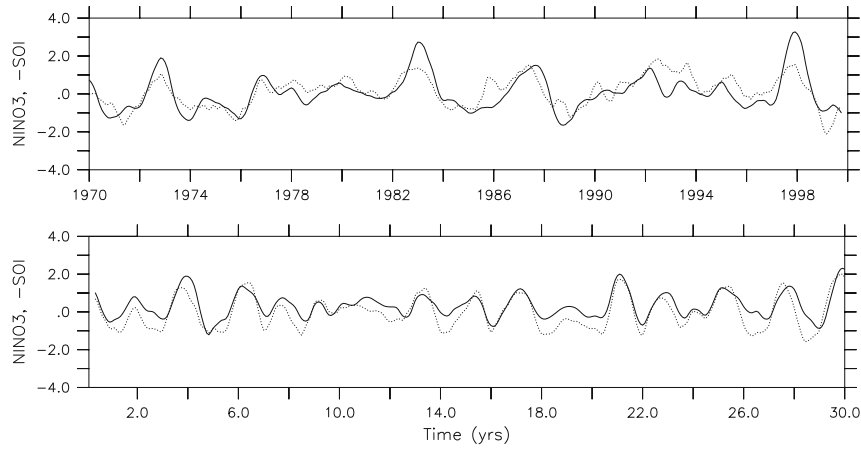


Fig. 7. Regression patterns between model anomalies and NINO3. (a) Surface air temperature, contour interval  $c = 0.2$  °C. (b) Sea level pressure,  $c = 0.3$  hPa. (c) surface winds in m/s. (d) vertical velocity,  $c = 0.1 \times 10^{-3}$  m/s.

The Southern Oscillation Index (SOI), defined as the normalized SLP difference anomaly between Darwin and Tahiti is widely used to monitor the ENSO cycle (Ropelewski and Jones, 1987). Positive SAT anomalies in the eastern Tropical Pacific (Fig. 7, panel a)) lead to negative SLP anomalies at the same location and a large scale pressure gradient to the western Tropical Pacific (Fig. 7, panel b)). As a result, the SOI has negative values during El Niño and high values during La Niña. In the NCEP data, SOI and NINO3 time series are closely related (Fig. 8) with a correlation coefficient  $r = -0.5$

for monthly mean values and the highest correlation ( $r = -0.72$ ) when both time series are smoothed with a running mean of 13 month.

The model reproduces the SLP response to prescribed SST anomalies and also the high correlation between SOI and NINO3 (Fig. 8) with  $r = -0.8$  ( $-0.9$ ) for (smoothed) monthly mean values. The amplitude of the SLP difference between Tahiti and Darwin in CLIMBER-3 $\alpha$  varies around its mean value of 6.3 hPa (NCEP: 5.2 hPa) with a standard deviation of 1.5 hPa (NCEP: 1.6 hPa).



**Fig. 8.** NINO3 time series (solid) and negative SOI (dotted) from NCEP (top) and model (bottom). Both monthly time series are smoothed with a running mean of 6 month.

The natural SLP variability is thus well represented in the model, at least in the Tropical Pacific domain. This represents a good test for the model, which is able to simulate the correct large scale response to the imposed SST variability. At the same time, the higher correlation shows that the model exhibits a more linear behavior than the real world and that the introduced ENSO mode is the only source of variability.

**3.2. Teleconnections**

In general, the model dynamics follow the prescribed SST and are able to reproduce the main atmospheric features of ENSO-related variability in the forcing domain. Outside of the Tropical Pacific however, the transport of the ENSO-signal is strongly damped, especially in meridional direction. The simplified atmospheric model dynamics of CLIMBER-3 $\alpha$  do not properly simulate tropical–extratropical teleconnections and the introduced ENSO variability stays largely confined to the forcing region.

The regression of the NINO3 onto the precipitation time series in the model reproduces the main feature of the reanalysis data of a positive regression in the central and east Tropical Pacific (Fig. 9). Negative regression coefficients outside of this domain are only visible in the model which can be explained by the lack of other variability.

**3.2.1. Atlantic freshwater budget**

The ENSO-related precipitation pattern in the model reproduces a bipolar structure of positive anomalies over the eastern Pacific

and negative anomalies over Central America and the Atlantic as found in observations. The presence and possible climatic importance of an ENSO-related exchange of freshwater between Pacific and Atlantic basin has been shown by Schmittner et al. (2000). Furthermore, model experiments by Schmittner et al. (2000), Latif et al. (2000) have shown a mechanism linking changes in the trans-continental freshwater transport with changes in the strength of the Atlantic meridional overturning circulation. Com-

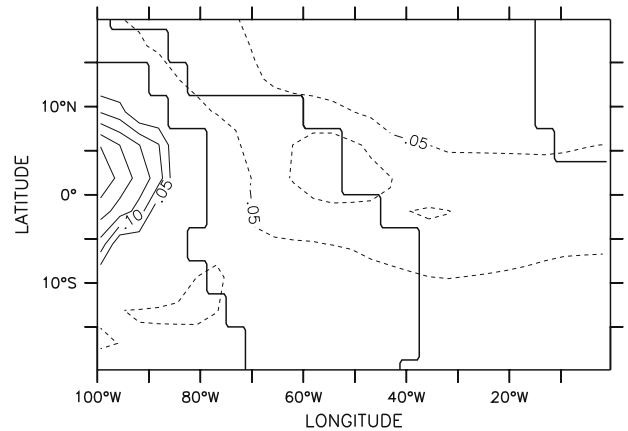


**Fig. 10.** Regression pattern between evaporation–precipitation and SOI. Contour interval is 0.05 m/yr. Compare with Fig. 1 in Schmittner et al. (2000).

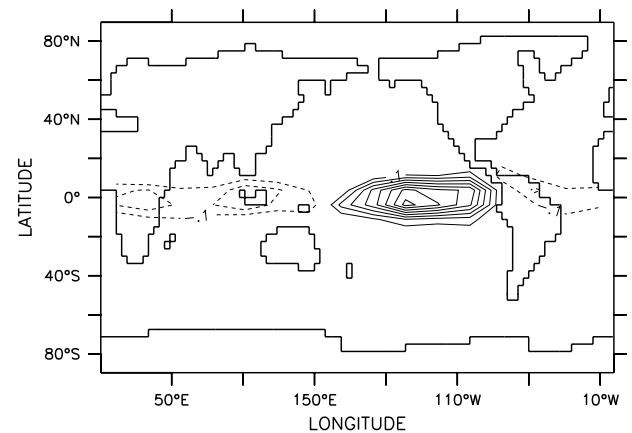
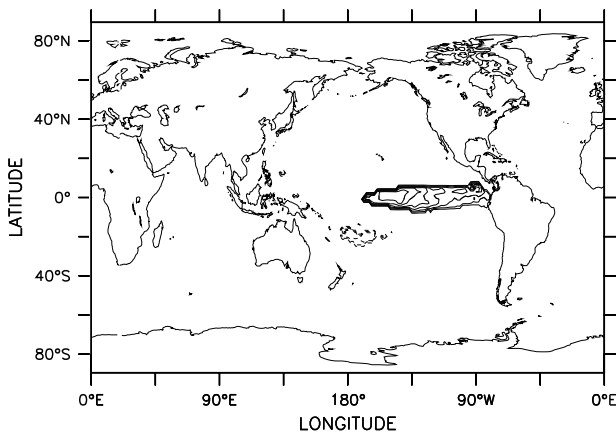


**Fig. 9.** Regression pattern between precipitation and NINO3 for NCEP (left) and Model (right). Contour interval is 0.2 mm/day.

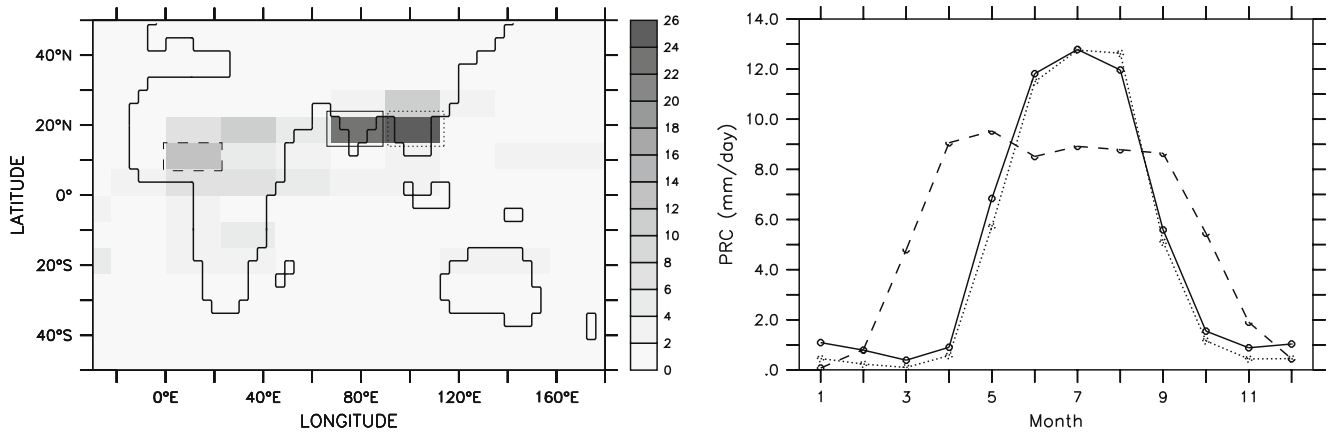


**Fig. 11.** Left: Monsoon regions in the model: West African monsoon (dashed, 0°–22.5°E, 7.5°–15°N), Indian monsoon (solid, 67.5°E–90°E, 15°N–22.5°N) and South-East Asian monsoon (dotted, 90°E–112.5°E, 15°N–22.5°N). The gray shading gives the variance of the seasonal cycle. Right: Seasonal cycle of monsoon rainfall for the West African monsoon (dashed), the Indian monsoon (solid) and the South-East Asian monsoon (dotted) in the control run.

parable to the analysis in Schmittner et al. (2000), we carried out a linear regression of evaporation minus precipitation against the SOI time series in the model (Fig. 10). The resulting pattern is dominated by the precipitation part (compare Fig. 9) and reproduces the bipolar structure across the American continent found in the reanalysis data.

The amplitude of the ENSO-related Atlantic freshwater anomaly in our model is  $-0.03$  Sv ( $1 \text{ Sv} = 10^6 \text{ m}^2 \text{ s}^{-1}$ ) for an increase of the SOI by one, which is smaller by a factor of 2 compared to the number derived by Schmittner et al. (2000) from reanalysis data.

A significant influence of ENSO-induced freshwater anomalies on the THC is only present when the ENSO model remains in constant El Niño-like conditions for several years which can occur during intermittent phases of the ENSO model (compare Fig. 5). The time scale of transport of ENSO-induced salinity anomalies from the Tropics to the northern Atlantic regions of deep water formation in the order of a decade is too long for an influence on THC strength under normal conditions (Mignot and Frankignoul, 2005; Goelzer et al., 2006).

### 3.2.2. Monsoon teleconnections

Although the strength of this correlation varies on a decadal time scale (Kucharski et al., 2007), ENSO is thought to have an influence on the Asian monsoon systems (e.g. Kumar et al. (2006)). This can be explained by anomalous subsidence over Asia as a result of the perturbed Walker circulation (Ropelewski and Halpert, 1987).

CLIMBER-3 $\alpha$  exhibits regions of monsoon activity in west Africa, the Indian Peninsula and South-East Asia (Fig. 11).

Due to the simplified atmospheric model dynamics in CLIMBER-3 $\alpha$ , however, ENSO-related subsidence anomalies (Fig. 7, panel d) are confined to the Tropical Indian Ocean. ENSO-related variations of the summer monsoon rainfalls thus reach only amplitudes of up to 4.5% of the seasonal cycle (Fig. 11) and do not show the expected correlation with the NINO3.

## 4. Discussion

We have presented a model setup which couples the ZC ENSO-model to the Earth system model of intermediate complexity CLIMBER-3 $\alpha$ . We show in how far ENSO variability can be introduced to an EMIC, which by itself exhibits no interannual variability. CLIMBER-3 $\alpha$  inherits the ENSO-related SST variability from the ZC model and can otherwise influence the ZC background state through modification of its long-term mean climate state. The fully

coupled model shows realistic ENSO-related variability of SST, SLP, and precipitation in the tropical band between 20°S and 20°N, in and close to the forcing domain. The representation of ENSO-related SLP variability in the model solely based on prescribed SST which results in a SOI variability comparable to observations is not trivial given the coarse and simplified atmospheric model. However, transport of the ENSO signal outside of the forcing domain is strongly damped, especially in meridional direction, thus preventing tropical–extratropical teleconnections. Introducing an improved statistical–dynamical atmospheric model (Petoukhov et al., 2003) or even a coarse resolution AGCM, may be a promising and necessary step in order to improve the representation of ENSO in the model. This limitation in the current model also inhibits the influence of ENSO on the Indian and South-East Asian monsoon systems through perturbation of the walker circulation, which is expected to suppress monsoon rains during El Niño. Instead we find a very weak reversed correlation compared to observations. We do find an ENSO-related modulation of the Atlantic freshwater budget, dominated by precipitation anomalies with a bipolar structure across the American continent. This link may be used to study the influence of long-term shifts in the ENSO cycle on the THC.

The influence of the ZC background state through changes in the long-term climate state of CLIMBER-3 $\alpha$  may be used to study the sensitivity of ENSO to a warming climate or other scenarios of past and future climate change.

## Acknowledgements

Thanks to Mark Cane for the model code and invaluable support with the ZC model. A.L. and H.G. were funded by the Gary Comer foundation.

## References

- AchutaRao, K., Sperber, K., 2006. ENSO simulation in coupled ocean–atmosphere models: are the current models better? *Climate Dyn.* 27 (1).
- Battisti, D., 1988. Dynamics and thermodynamics of a warming event in a coupled tropical atmosphere–ocean model. *J. Atmos. Sci.* 45 (20), 2889–2919.
- Battisti, D., Hirst, A., 1989. Interannual variability in a tropical atmosphere–ocean model: Influence of the basic state, ocean geometry and nonlinearity. *J. Atmos. Sci.* 46 (12), 1687–1712.
- Bjerknes, J., 1969. Atmospheric teleconnections from the equatorial pacific. *Monthly Weather Rev.* 97 (3), 163–172.
- Chen, D., Cane, M., Kaplan, A., Zebiak, S., Huang, D., 2004. Predictability of El Niño over the past 148 years. *Nature* 428, 733–736.
- Cheeto, T., Maqueda, M., 1997. Sensitivity of a global sea ice model to the treatment of ice thermodynamics and dynamics. *J. Geophys. Res.* 102, 12609.
- Ganachaud, A., Wunsch, C., 2000. Improved estimates of global ocean circulation, heat transport and mixing from hydrographic data. *Nature* 408, 453–456.

- Ganopolski, A., Petoukhov, V., Rahmstorf, S., Brovkin, V., Claussen, M., Eliseev, A., Kubatzki, C., 2001. CLIMBER-2: a climate system model of intermediate complexity. Part ii: model sensitivity. *Climate Dyn.* 17, 735.
- Gill, A.E., 1982. *Atmosphere–Ocean Dynamics*. Academic Press.
- Gnanadesikan, A., 1999. A simple predictive model for the structure of the oceanic pycnocline. *Science* 283, 2077–2079.
- Goelzer, H., Mignot, J., Levermann, A., Rahmstorf, S., 2006. Tropical versus high latitude freshwater influence on the Atlantic circulation. *Climate Dyn.* 27, 715–725.
- Hofmann, M., Maqueda, M.M., 2006. Performance of a second-order moments advection scheme in an ocean general circulation model. *J. Geophys. Res.* 111, C05006.
- Jin, F., 1997. An equatorial ocean recharge paradigm for ENSO. *J. Atmos. Sci.* 54 (7), 811–829.
- Kalnay, E. et al., 1996. The NCEP/NCAR 40-year reanalysis project. *Bull. Am. Meteorol. Soc.* 77, 437–471.
- Kucharski, F., Bracco, A., Yoo, J.H., Molteni, F., 2007. Low-frequency variability of the Indian monsoon–ENSO relationship and the tropical Atlantic: the weakening of the 1980s and 1990s. *J. Climate* 20 (16), 4255–4266.
- Kumar, K.K., Rajagopalan, B., Hoerling, M., Bates, G., Cane, M., 2006. Unraveling the mystery of Indian monsoon failure during El Niño. *Science* 314 (5796), 115–119.
- Latif, M., Roeckner, E., Mikolajewicz, U., Voss, R., 2000. Tropical stabilisation of the thermohaline circulation in a greenhouse warming simulation. *J. Climate* 13, 1809–1813.
- Levermann, A., Griesel, A., 2004. Solution of a model for the oceanic pycnocline depth: Scaling of overturning strength and meridional pressure difference. *Geophys. Res. Lett.* 31, L17302.
- Levermann, A., Schewe, J., Montoya, M., 2007. Lack of bipolar see–saw in response to Southern Ocean wind reduction. *Geophys. Res. Lett.* 34, L12711.
- Mignot, J., Frankignoul, C., 2005. On the variability of the Atlantic meridional overturning circulation, the NAO and the ENSO in the Bergen Climate Model. *J. Climate* 18, 2361–2375.
- Mignot, J., Levermann, A., Griesel, A., 2006. A decomposition of the Atlantic Meridional Overturning Circulation into physical components using its sensitivity to vertical diffusivity. *J. Phys. Oceanogr.* 36, 636–650.
- Montoya, M., Levermann, A., 2008. Surface wind stress threshold for glacial Atlantic overturning. *Geophys. Res. Lett.* 35, L03608.
- Montoya, M., Griesel, A., Levermann, A., Mignot, J., Hofmann, M., Ganopolski, A., Rahmstorf, S., 2005. The earth system model of intermediate complexity CLIMBER-3 $\alpha$ . Part I: description and performance for present day conditions. *Climate Dyn.* 25, 237–263.
- Neelin, J., Battisti, D., Hirst, A., Jin, F., Wakata, Y., Yamagata, T., Zebiak, S., 1998. ENSO theory. *J. Geophys. Res.* 103, 14290.
- Pacanowski, R., Griffies, S., 1999. *The MOM-3 Manual*. Techn. Ber. 4. NOAA/Geophysical Fluid Dynamics Laboratory, Princeton, NJ, USA.
- Petoukhov, V., Ganopolski, A., Brovkin, V., Claussen, M., Eliseev, A., Kubatzki, C., Rahmstorf, S., 2000. CLIMBER-2: a climate system model of intermediate complexity. Part I: model description and performance for present climate. *Climate Dyn.* 16, 1.
- Petoukhov, V., Ganopolski, A., Claussen, M., 2003. POTSDAM – a set of atmosphere statistical–dynamical models: theoretical background. PIK Report, 81. Potsdam Institute for Climate Impact Research, Potsdam, Germany.
- Picaut, J., Masia, F., du Penhoat, Y., 1997. An Advective–Reflective Conceptual Model for the Oscillatory Nature of the ENSO. *Science*, 277.
- Prather, M., 1986. Numerical advection by conservation of second-order moments. *J. Geophys. Res.* 91, 6671.
- Reynolds, R.W., Smith, T.M., 1994. Improved global sea surface temperature analyses using optimum interpolation. *J. Climate* 7, 928–948.
- Ropelewski, C., Halpert, M., 1987. Global and regional scale precipitation patterns associated with the El Niño/Southern Oscillation. *Monthly Weather Rev.* 115, 1606–1626.
- Ropelewski, C., Jones, P., 1987. An extension of the Tahiti–Darwin Southern Oscillation Index. *Monthly Weather Rev.* 115, 2161–2165.
- Schewe, J., Levermann, A., accepted for publication. The role of meridional density gradients for a wind-driven overturning. *Climate Dyn.* doi:10.1007/s00382-009-0572-1.
- Schmittner, A., Appenzeller, C., Stocker, T., 2000. Enhanced Atlantic freshwater export during El Niño. *Geophys. Res. Lett.* 27 (8), 1163–1166.
- Suarez, M., Schopf, P., 1988. A delayed action oscillator for ENSO. *J. Atmos. Sci.* 45 (21), 3283–3287.
- Talley, L., Reid, J., Robbins, P., 2003. Data-based meridional overturning streamfunctions for the global oceans. *J. Climate* 16, 3213–3226.
- Timmermann, A., An, S.-I., Krebs, U., Goosse, H., 2005. ENSO suppression due to weakening of the North Atlantic thermohaline circulation. *J. Climate* 18 (16), 3122–3139.
- Trenberth, K., Olson, J., Large, W., 1989. A global ocean wind stress climatology based on ECMWF analyses. Tech. Rep. NCAR/TN-338+STR. National Center for Atmospheric Research, Boulder.
- Tziperman, E., Zebiak, S., Cane, M., 1997. Mechanisms of seasonal–ENSO interaction. *J. Atmos. Sci.* 54, 61–71.
- von Storch, H., Zwiers, F., 1999. *Statistical Analysis in Climate Research*. Cambridge University Press.
- Wang, C., 2001. A unified oscillator model for the El Niño/Southern Oscillation. *J. Climate* 14, 98–115.
- Zebiak, S.E., Cane, M.A., 1987. A model El Niño/Southern Oscillation. *Monthly Weather Rev.* 115, 2262–2278.